ELSEVIER

Formation of perfused, functional microvascular tubes in vitro

Kenneth M. Chrobak, Daniel R. Potter, Joe Tien *

Department of Biomedical Engineering, Boston University, 44 Cummington Street, Boston, MA 02215, USA

Abstract

This work describes the formation, perfusion, and maturation of three-dimensional microvascular tubes in vitro. These tubes consisted of confluent monolayers of human endothelial cells that lined open, cylindrical channels within collagen gels. Perivascular cells could be directly embedded within the gels or added after endothelial cells grew to confluence. The tubes spanned the entire 5–7 mm extent of the gels; their diameters initially ranged from 55 to 120 μm and increased to 75–150 μm after maturation. Endothelial tubes displayed a strong barrier function over 5 days, resisted adhesion of leukocytes, and reacted quickly to inflammatory stimuli by breakdown of the barrier and support of leukocyte adhesion. These tubes resembled venules and "giant" capillaries in both their cellular organization and function, and we believe that they will serve as useful in vitro models of inflammation under constant perfusion.
© 2006 Elsevier Inc. All rights reserved.

Introduction

In vitro studies of microvascular function normally examine the behavior of microvascular cells cultured on two-dimensional (2D) substrates or within three-dimensional (3D) gels (Folkman et al., 1979; Albelda et al., 1988; Kvietys and Granger, 1997; Madri et al., 1988; Jalali et al., 2001). While these cultures have successfully modeled several microvascular behaviors, they do not easily combine lumenal flow with a 3D tubular organization. Thus, modeling of complex behaviors – in particular, the interplay between flow and the inflammatory response – remains challenging in vitro. In this article, we address these issues by introducing a method to form open tubes of microvascular cells in a collagen gel. These tubes reproduce the 3D endothelial organization in microvessels and are readily perfused. They are stable for several days, exhibit a strong barrier function, react to inflammatory stimuli, and support the adhesion of leukocytes under shear. We believe that these constructs represent the first examples of perfused, functional in vitro microvascular tubes and expect that they will serve as convenient models for studies of microvascular functions that require the presence of lumenal flow.

Methods to form microvascular tubes in vitro generally rely on the self-organization of endothelial cells (ECs), by themselves or with mesenchymal cells, in biological gels such as type I collagen or Matrigel (Montesano et al., 1983; Darland and D'Amore, 2001). Previous studies have shown that ECs seeded on or embedded in gels can reorganize into structures that possess open lumens (Montesano et al., 1983; Montesano and Orci, 1985). To our knowledge, none of these studies has demonstrated a functional interconnection between individual endothelial segments that allows perfusion of the tubes across the entire extent of the gels.

Our approach cultures ECs on the surfaces of ∼100-μm-diameter open channels that span entire collagen gels. Because channels already exist within the gels, perfusion is readily established upon seeding, and introduction of agents (agonists, cells) to probe microvascular function is straightforward. In spirit, our strategy resembles one that was previously used to engineer small-diameter arteries (Weinberg and Bell, 1986). There, ∼5-mm-diameter tubes were created by casting collagen and smooth muscle cells in an annular mold; these tubes were lined with bovine aortic ECs after removal of the mold. A recent study has applied a similar strategy to create ∼100-μm-diameter tubes of smooth muscle cells (Neumann et al., 2003).

Here, we describe the construction of microvascular tubes of endothelial cells with final diameters ranging from 75 to

---

* Corresponding author. Fax: +1 617 353 6766.
 E-mail address: jtien@bu.edu (J. Tien).

150 μm. Minimization of cell-induced "defects" as these tubes matured over time was essential to obtain stable structures. Specifically, we optimized the preparation of the collagen gels to minimize contraction and invasion of the gels by ECs that lined the lumens. Tubes in these gels were stable for at least 1 week under perfusion conditions that resembled those in venules in vivo (i.e., average lumenal pressure of ~10 mm Hg and shear stress of ~10 dyn/cm^2). In the absence of inflammatory agonists, the basal barrier function and adhesiveness of the endothelial layer in these tubes mimicked those of venules in vivo. Addition of the agonists histamine, thrombin, or tumor necrosis factor-α (TNF-α) resulted in breakdown of the barrier and/or a sharp increase in adhesiveness to leukocytes.

Materials and methods

Cell culture

This study used four types of cells: human umbilical vein endothelial cells (HUVECs), human dermal microvascular endothelial cells (HDMECs), human perivascular cells (PCs), and transformed human neutrophil-like HL-60 cells. In theory, tubes made from HDMECs ("HDMEC tubes") should behave more closely to actual microvessels than those made from HUVECs ("HUVEC tubes") should. In practice, however, all commercially available HDMECs contain a sizeable fraction of cells that is lymphatic in origin (Podgrabinska et al., 2002; Kriehuber et al., 2001; data not shown); the long-term stability of cultures sorted to remove lymphatic HDMECs is unclear (Groger et al., 2004). HUVECs, in contrast, do not express lymphatic markers (data not shown). Thus, we used both HDMECs and HUVECs in our engineered structures, although neither cell type may be ideal.

HUVECs (Cambrex) were cultured at 37°C in 5% CO$_2$ in M199 (Cambrex) that was supplemented with 20% heat-inactivated fetal bovine serum (FBS; GIBCO), 2 mM L-glutamine, 100 U/mL penicillin, 100 μg/mL streptomycin (1% GPS; GIBCO), 25 μg/mL endothelial cell growth supplement (ECGS; Biomedical Technologies), 5 U/mL heparin (Sigma), and 0.2 mM L-ascorbic acid 2-phosphate (Sigma). HUVECs were routinely passaged at a 1:8 ratio onto gelatin-coated tissue culture plates and were discarded after passage 9. HDMECs from neonatal foreskin (Cascade Biologics) were cultured at 37°C in 5% CO$_2$ in MCDB 131 (GIBCO) and supplemented with 10% FBS, 1% GPS, 1 μg/mL hydrocortisone (Sigma), 80 μM dibutyryl cAMP (Sigma), 25 μg/mL ECGS, 2 U/mL heparin, and 0.2 mM L-ascorbic acid 2-phosphate. HDMECs were routinely passaged at a 1:4 ratio onto gelatin-coated tissue culture plates and were discarded after passage 6. Dispase (1 U/mL in phosphate-buffered saline (PBS); GIBCO) was used instead of trypsin to detach ECs from culture plates because trypsin may cleave protease-activated receptors on ECs, leading to expression of adhesion molecules such as P-selectin (Coughlin, 2000; Collins et al., 1993).

Because human PCs are not commercially available as pure cultures, we isolated them by culturing HDMECs (VEC Technologies) under conditions that favored the growth of mesenchymal cells: culturing passage 4 HDMECs in M199 supplemented with 20% FBS, 1% GPS, 25 μg/mL ECGS, and 5 U/mL heparin allowed a sub-population of spindly cells to overgrow the ECs within 1 week. Confluent cultures of these cells exhibited the "hill-and-valley" morphology typical of cultures of smooth muscle cells (Chamley-Campbell et al., 1979) but expressed smooth muscle markers such as smooth muscle actin in only ~20% of cells (data not shown). We believe that these cells most likely represent mural cells that co-purified with HDMECs during primary isolation (Gitlin and D'Amore, 1983; Richard et al., 1998). PCs were weaned into DMEM supplemented with 10% CS and 1% GPS and were routinely passaged at 1:4 with cold trypsin.

HL-60 cells (ATCC) were cultured at 37°C in 5% CO$_2$ in RPMI 1640 (GIBCO) supplemented with 10% FBS and 1% GPS (Collins, 1978) and were routinely passaged at a 1:4 ratio from non-adherent cultures.

Construction of microvascular tubes

Fig. 1 outlines the strategy we used to form EC-lined tubes in collagen. First, standard lithographic techniques generated a sturdy "housing" of silicone rubber that eventually served as a mechanical support to the gel. Briefly, patterned irradiation of a 1-mm-thick layer of photoresist (SU-8 50; MicroChem) and subsequent development with propylene glycol monomethyl ether acetate yielded a patterned wafer with raised features of 1 mm × 1 mm × 1 cm. Casting and curing a liquid silicone elastomer (Sylgard 184; Dow Corning) against the patterned wafer created a silicone replica with 1-mm-deep indentations.

To make a single tube, we cut 6-mm-diameter holes in the silicone, sterilized the silicone with 70% ethanol, and placed it indentation-side down on a plastic or glass substrate. The inner surface of the silicone housing was coated with 10 μg/mL fibronectin (BD Biosciences) for 40 min at 23°C to promote adhesion of collagen to the silicone. We coated a 120-μm-diameter, 15-mm-long stainless steel needle (Seirin needles; Health Point Products) with 1% bovine serum albumin (BSA; Calbiochem) for 40 min at 23°C and then carefully threaded it between the housing and the substrate. The needle did not contact any walls of the silicone or substrate. Addition of neutralized liquid collagen into the silicone housing surrounding the needle, gelation of collagen for 2 h at 19–37°C, and removal of the needle yielded 120-μm-diameter channels in collagen gel. Neutralized collagen solution consisted of 15 μL 10× PBS (GIBCO), 4.8 μL H$_2$O, 6.5 μL 0.2 M NaOH (Sigma), 1.2 μL 7.5% sodium bicarbonate (GIBCO), and 122.7 μL collagen stock (7.9 mg/mL type I collagen from rat tail, lot 15426; BD Biosciences), which yielded a final collagen concentration of 6.5 mg/mL at a pH of 7.0–7.5. To obtain collagen with lower concentrations, collagen stock was diluted with cold 0.02 M acetic acid before neutralization. All silicone housings were sealed with additional silicone to ensure that the seal between housing and substrate could withstand pressures up to 50 cm H$_2$O.

Introduction of a suspension of ECs into the collagen tube (~10^7 cells/mL in culture media supplemented with 4% dextran (70 kDa; Sigma)) allowed a sub-confluent layer of ECs to attach to the inner surface of the collagen. Dextran increased the viscosity of the media to enable fine control over seeding density; for 4% dextran, measured viscosities at 37°C were 1.63 ± 0.07 cP ($n = 6$). Five minutes after seeding, a low flow (~3 μL/min) of media flushed unattached cells from the collagen. We deliberately seeded ECs at 20–50% confluence because higher seeding densities led to severe contraction and/or invasion of the tube by ECs as they spread out. To seal the channel and introduce flow, we cast a "lid" of silicone that contained two 50-cm-long pieces of sterile polyethylene tubing (PE50; Intramedic) spaced to align with the two holes in the housing. Once placed on the housing, the lid sealed passively to form a water-tight bond. Introduction of dextran-containing media from a culture dish through the inlet tubing allowed media to flow under gravity into the inlet well and through the endothelial tube and to exit via the outlet tubing into a second dish. Here, the addition of dextran serves to lower the flow rate. We manually recirculated media from the lower to the higher dish once or twice per day as needed and replaced the media every 2 days. In some cases, media with protease inhibitors or reduced amounts of growth factors were added at the day of seeding (day 0) or 2–3 days post-seeding, respectively. Fig. 1 shows representative images of a bare collagen tube and a HUVEC tube after cells grew to confluence; cross-sectional views verify that the channels were initially cylindrical.

We used two different methods to generate tubes that incorporated both HDMECs and PCs. The first method added a suspension of PCs in ~5 μL of HDMEC culture media to neutralized liquid collagen before gelation around needles; this procedure evenly distributed PCs within the collagen at ~10^5 cells/mL. The collagen with suspended cells was gelled at 23°C for 10 min and then at 37°C for an additional 2 h. Removal of needles and addition of HDMECs used the same procedure as that described for tubes with only ECs. The second method seeded PCs directly into endothelial tubes after seeded ECs had grown to confluence. To visualize the relative locations of HDMECs and PCs, we labeled PCs with 10 μM CellTracker Red (CMTPX; Molecular Probes) in DMEM for 30 min at 37°C before use. To visualize the completeness of the HDMEC monolayer, we stained tubes for the endothelial cell marker CD31: tubes were fixed by perfusion with 4% paraformaldehyde for 1 h, blocked in 20% goat serum (GS) for 30 min, incubated in mouse anti-CD31 antibody (clone WM59, 2 μg/mL in 20% GS; Sigma) for 30 min, washed in 20% GS, incubated in Alexa-Fluor-488-conjugated goat anti-mouse antibody (15 μg/mL in 20% GS; Molecular Probes) for 30 min, and washed in PBS. Stained tubes were
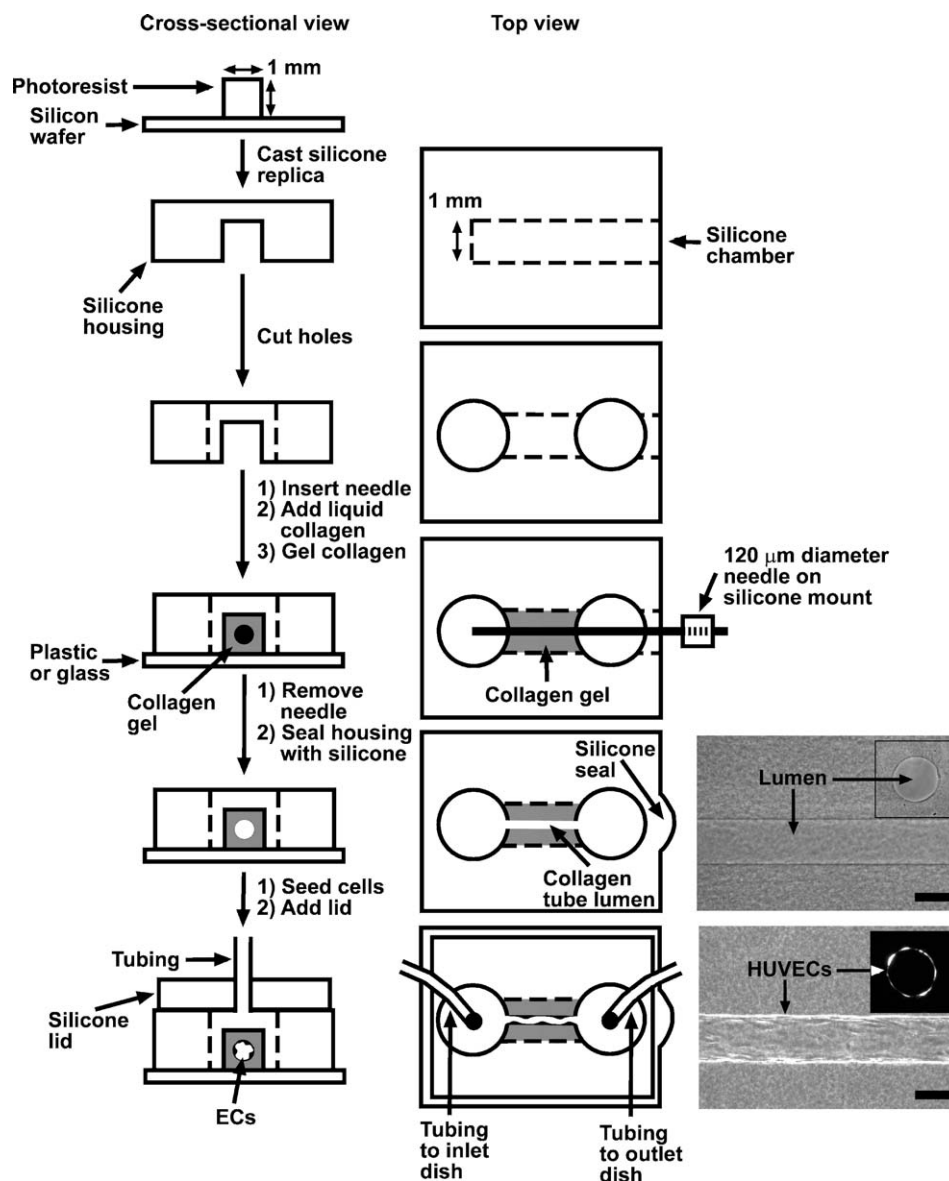
Fig. 1. Schematic diagram of the assembly of an endothelial tube. A silicone housing with two holes served as a mechanical support. Placement of the housing on a substrate defined a millimeter-scale chamber, through which we suspended a needle using a silicone mount. We added collagen into the chamber to surround the needle and allowed the liquid to gel. Removal of the needle and sealing of the housing yielded a collagen tube that contacted the two holes. Seeding of ECs through the tube, addition of a lid with inlet and outlet tubing, and establishment of flow completed the process. Shown are top and cross-sectional phase-contrast images of a bare collagen tube and one lined by a confluent layer of HUVECs (2 days post-seeding). HUVECs were labeled with CellTracker Green before seeding; the cross-sectional view of the HUVEC tube is a fluorescence image. Scale bars refer to 100 μm.

imaged with a Zeiss Axiovert 200 M inverted microscope coupled to an Apotome structured-illumination device to generate confocal-like images. For each optical section, this device projected a fine grid onto the focal plane of the objective and took three images with the grid at three different locations; mathematical recombination of these images using Axiovision 4.4 software generated an image in which the projection of the grid was no longer present and in which low-frequency signal (i.e., out-of-focus light) was greatly reduced (Neil et al., 1997). We used a Plan-Apo 10× objective (NA 0.45, Zeiss) to generate optical sections centered at the mid-planes of stained tubes.

Analysis of contraction and invasion of collagen by ECs

Phase-contrast images of microvascular tubes were captured with an AxioCam MRm camera (1300 × 1030 resolution) using a Plan-Neo 10× objective (NA 0.30, Zeiss). Because each tube was 6–7 mm long, analysis required stitching of images; we used Adobe Photoshop 6.0 for this purpose. For each tube, widths were measured at least ten points along its axis to yield a mean and standard deviation for an individual tube. Data from multiple tubes were combined to yield a mean and standard deviation for each experimental condition (see Statistical analysis). Measurement of widths for HUVEC and HDMEC tubes took place at 2 h and 1–2 days post-seeding, respectively. The numbers of invasive ECs per millimeter tube length were found by counting all cells that penetrated the collagen, whether they were completely encased in the gel or only extended small filopodia into it. In all images in the figures, flow occurred from left to right.

Embedding and sectioning

To obtain cross-sectional images of tubes, we used polyethylene glycol (PEG) as an embedding medium (Klosen et al., 1993) since PEG-based sections

preserve morphology better than paraffin-based or frozen sections do (Holtham and Slepecky, 1995). Briefly, we fixed gels by removing the silicone lids and perfusing tubes with 4% paraformaldehyde for 1 h at 23°C. The silicone housings were then carefully removed, and the remaining collagen was washed with PBS and dehydrated in sequential steps of 25%, 50%, 75%, and 100% PEG 1000 (Sigma) at 60°C for 1 h each. Fresh 100% PEG (melted at 60°C) was then added, and the sample was allowed to harden under vacuum overnight at room temperature. The PEG block was sliced into 10-μm-thick sections using a rotary microtome (HM 355S; Microm) and transferred onto coverslips using an agarose slab as a carrier (Gao and Godkin, 1991). Although epoxy-based embedding media also yielded sections with well-preserved morphologies, we found that PEG blocks were much easier to ribbon and provided more useable sections per block.

Permeability assays

To determine the permeability of EC tubes (with and without PCs), we removed the silicone lids and perfused HDMEC tubes with a solution of Alexa-Fluor-488-labeled BSA (50 μg/mL in media used for HDMEC tubes; Molecular Probes) or Alexa-Fluor-488-labeled 3 kDa dextran (5 μg/mL in media used for HDMEC tubes; Molecular Probes) in an environmental chamber set at 37°C. Fluorescence images were captured every minute for 20 min with the Plan-Neo 10× objective, corrected for non-uniformities in field intensity, and combined to generate movies of basal and agonist-induced leakage. We calculated the permeability coefficient P from the equation $P = (1/\Delta I) \, (\mathrm{d}I/\mathrm{d}t)_0 \, (r/2)$, where ΔI is the increase in total fluorescence intensity upon adding labeled BSA, $(\mathrm{d}I/\mathrm{d}t)_0$ is the initial rate of increase in
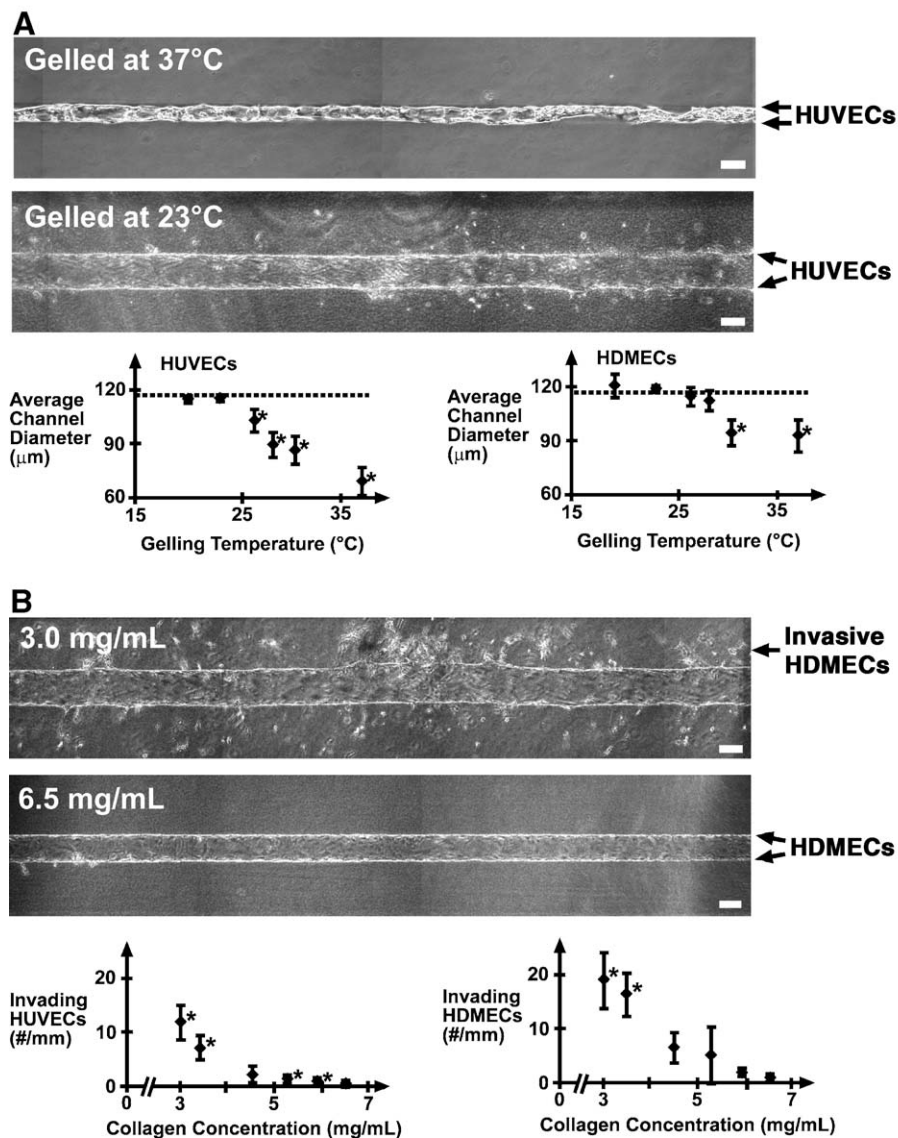

Fig. 2. Effects of gelling temperature and collagen concentration on deformation and invasion of tubes. (A) Composite images of HUVEC tubes in 3.0 mg/mL collagen gelled at 37°C and 23°C. The 37°C tube shown here contracted and collapsed by day 2 after seeding. The 23°C tube did not contract initially, but after reaching confluence, HUVECs began to invade the surrounding collagen matrix. Plots of average diameters versus temperature of gelation show that gelling temperatures above 23–27°C lead to significant contraction (*) compared to unseeded collagen tubes (116 ± 1 μm; dashed lines). At all gelling temperatures, EC tubes were significantly rougher than bare tubes. (B) Composite images of HDMEC tubes in 3.0 and 6.5 mg/mL collagen gelled at 23°C. Many more ECs invaded the 3.0 mg/mL tube than the 6.5 mg/mL one. Plots of EC invasion versus collagen concentration show that collagen concentrations below 4.0 mg/mL lead to significant differences (*) in cellular invasion compared to 6.5 mg/mL tubes. For all HUVEC tubes in ≤6.0 mg/mL collagen, numbers of invading cells were significantly more varied than for HUVEC tubes in 6.5 mg/mL collagen. For all HDMEC tubes in ≤5.0 mg/mL collagen, numbers of invading cells were significantly more varied than for HDMEC tubes in 6.5 mg/mL collagen. Scale bars refer to 100 μm.

intensity as BSA diffuses out of the tube into the surrounding gel, and r is the radius of the tube (Huxley et al., 1987; Yuan et al., 1992, 1993). We estimated ΔI by measuring the average intensity outside the tube immediately after addition of labeled BSA, multiplying this intensity over the area of the image, and subtracting this product from the total intensity of the image. We estimated $(dI / dt)_0$ by plotting the total intensity of the image versus time and finding the slope during the first 3 min. These measurements required the use of #1 1/2 coverslips as substrates to decrease background fluorescence. As controls, we checked that (1) the fluorescence signal was proportional to BSA concentration in the range of 0.2–50 μg/mL, and (2) changing the plane of focus led to <5% variation in total intensity.

In some tubes, histamine (Sigma) was perfused at 100 μM for 5 min prior to adding labeled BSA; histamine was kept in the perfusing media throughout the measurements. Because dibutyryl cAMP (an additive in the HDMEC culture media) can antagonize the effects of histamine (Moy et al., 1993), in some samples, we removed the cAMP analog from the media 24 h before removing the lid and adding histamine. To block the effects of histamine, we added the H1 receptor antagonist pyrilamine (Sigma) at 100 μM for 5 min before adding histamine; pyrilamine was kept in the perfusing media throughout the measurements. In other samples, 10 U/mL thrombin (Sigma) was added along with labeled BSA with and without dibutyryl cAMP.

HL-60 cell adhesion assays

To determine whether ECs in tubes are in a quiescent state and whether they respond to cytokines, we measured the adhesion of neutrophil-like HL-60 cells (Collins et al., 1978; Hauert et al., 2002) to HUVEC tubes with and without recombinant human TNF-α (R&D Systems). HL-60 cells were fluorescently labeled in RPMI 1640 with 10 μM CellTracker Green for 30 min at 37°C, washed, and re-suspended at 10^6 cells/mL in M199 with 20% FBS, 1% GPS, and 4% dextran.

We removed the silicone lids covering HUVEC tubes and allowed 60 μL of HL-60 suspension to flow through each tube for 10 min. Samples were used only if the flow rate exceeded 1 μL/min (corresponding to a shear stress of ≤0.8 dyn/cm²). Following exposure to HL-60 cells, tubes were washed with M199 supplemented with 20% FBS, 1% GPS, and 4% dextran for 10 min to remove any HL-60 cells that did not attach firmly to ECs. The number of adherent HL-60 cells per tube was determined from fluorescence images of the tubes; regions within 1 mm of either end were not counted since we often observed anomalously high densities of adherent cells (>40 cells/mm) along these segments.

To activate HUVEC tubes, we perfused them with 100 ng/mL TNF-α in media without ECGS and heparin for 4 h before removal of their lids and washed them with this media for 10 min before adding HL-60 cells. To inhibit the adhesion of HL-60 cells, we perfused tubes with mouse antibody to E-selectin (clone 1.2B6, used at 4 μg/mL in HUVEC tube media; Sigma) for 20 min at 37°C after the TNF-α treatment and prior to addition of HL-60 cells. In some cases, HL-60 cells were exposed to a mouse antibody to CD18 (clone L130, used at 3 μg/mL; BD Pharmingen) at 37°C for 20 min before addition to clone 1.2B6-treated tubes.

Etching needles

Needles were partially submerged in a solution of nickel etchant (Transene Corporation) with ultrasonic agitation at 23°C. The etch rate was ~10 μm/min. After etching, needles were washed thoroughly with deionized H_2O and used to generate tubes with diameters less than 120 μm using the same procedure described for unetched needles.

Statistical analysis

Data are reported as means ± standard deviations. Comparisons between means (Figs. 2A, B, and 4) used Student's two-tailed t test for equal means in samples with unequal variances. For analysis of tube diameters, we first determined a mean and standard deviation for each individual tube and then calculated a weighted mean for all tubes at a particular experimental condition. Likewise, we calculated a weighted standard deviation by using means and standard deviations for each tube (Crow et al., 1960). Comparisons of variances

(i.e., comparisons of the "roughness" of tubes) used Wilcoxon's Sum of Ranks test. Differences were considered significant when $P < 0.05$.

Results

Effects of temperature and collagen concentration on deformation in HUVEC and HDMEC tubes

Bare collagen tubes had uniform diameters of 116 ± 1 μm ($n = 7$) over their entire ~6 mm lengths (Fig. 1); the standard deviation combines both the variation within a single tube and between tubes. These diameters did not change after 5 days of perfusion with an inlet pressure of 16 cm H_2O, an outlet pressure of 11 cm H_2O, and shear stress of 10 dyn/cm². We estimated shear stress with the formula $\tau = 4Q\mu/\pi r^3$, which describes flow through a cylindrical pipe. Here, τ is the shear stress, Q is the measured volumetric flow (~0.4 mL/h), μ is the viscosity of dextran-containing media (1.63 ± 0.07 cP; $n = 6$), and r is the radius of the collagen tube (58 ± 0.5 μm). We chose to use experimentally measured flow rates rather than pressures to determine the shear stress to avoid errors due to unknown pressure losses along the polyethylene tubing that connected dishes of media to the collagen tubes.

Seeding either HUVECs or HDMECs into 3.0 mg/mL collagen tubes gelled at 37°C led to the emergence of three types of "defects": contraction, invasion, and expansion. These behaviors appeared at characteristic, overlapping intervals after seeding. At days 1–2 (i.e., 1–2 days post-seeding), prior to reaching confluence, tubes often severely contracted, most likely from cell-induced forces (Fig. 2A). At days 2–3, just after reaching confluence, many ECs invaded the gel (Fig. 2B). At days 3–7, tubes expanded to much larger diameters (150–300 μm) and stabilized at this larger size. We chose to address these deformations in their order of appearance, focusing first on contraction, then cellular invasion, and finally expansion, and minimized them by optimizing the conditions of gelation and culture conditions.

To minimize contraction of tubes at days 1–2, we varied the temperature of gelation of the collagen. Gelation at lower temperatures tends to yield gels that have thicker fibrils (Williams et al., 1978; Wood and Keech, 1960). With thicker fibrils, these gels may deform less. Thus, we examined the contraction of tubes made from collagen gelled between 37°C and 19°C (at lower temperatures, the gels did not form consistently). Contraction of 3.0 mg/mL collagen that was gelled at 37°C and seeded with ECs was substantial, especially when HUVECs were seeded. Tubes contracted to 70 ± 10 μm ($60 \pm 8\%$ of the initial diameter; $n = 3$) when seeded with HUVECs and to 97 ± 10 μm ($83 \pm 8\%$; $n = 3$) when seeded with HDMECs. Moreover, the walls of these tubes were highly uneven and the tubes no longer resembled cylinders by days 1–2. In some cases, tubes of HUVECs contracted so much that flow ceased; HUVECs in these tubes invariably died by day 2.

In contrast, lower temperatures of gelation led to decreased contraction (Fig. 2A). In collagen tubes gelled at 23°C and below, contraction was nearly negligible for both HUVEC (114 ± 2 μm, $98 \pm 2\%$, $n = 3$) and HDMEC (121 ± 2 μm,

104 ± 2%, n = 3) tubes. The gels in these samples were noticeably coarser than those gelled at 37°C, which appears to reflect the thicker fibers in gels formed at lower temperatures. Since no additional decrease in contraction was found at temperatures below 23°C, we selected 23°C as the optimized temperature for subsequent experiments. Even at this gelation temperature, however, both HUVEC and HDMEC tubes were significantly rougher than a bare collagen tube (Fig. 2A); standard deviations of the widths along the seeded tubes were ~5 μm.

To minimize invasion of gels at days 2–3, we varied the concentration of collagen. An increase in the collagen concentration should decrease invasion by decreasing the pore size of the gel. In tubes in 3.0 mg/mL collagen, 12 ± 3 HUVECs/mm (n = 3) and 19 ± 6 HDMECs/mm (n = 5) invaded into the collagen by days 5–6 and days 2–3, respectively (Fig. 2B). The lumenal walls clearly deformed as ECs migrated into the collagen. At higher concentrations of collagen, the numbers of invading cells were lower, until nearly negligible values were observed for the highest concentration used, 6.5 mg/mL (0.2 ± 0.1 HUVECs/mm, n = 8; 0.7 ± 0.7 HDMECs/mm, n = 8). Fig. 2B shows that even a 20% increase in collagen concentration was enough to greatly reduce EC invasion. We chose 6.5 mg/mL as the optimized concentration for all subsequent experiments; in theory, higher concentrations should reduce invasion further.

In HUVEC and HDMEC tubes in optimized collagen (6.5 mg/mL, gelled at 23°C), the tubes did not contract and cells rarely invaded the gels. Most (>90%) tubes eventually expanded between days 3 and 7: HUVEC tubes enlarged to 151 ± 6 μm near the inlet and tapered to 142 ± 12 μm (n = 8) near the outlet of the tube. HDMEC tubes enlarged to

151 ± 3 μm at the inlet and tapered to 131 ± 7 μm (n = 8) at the outlet. Thus, the stable shape of these tubes appears to be a slightly tapering cone. In a small subset (<10%) of tubes, cells detached as a sheet from the collagen for unknown reasons.

Addition of a broad-spectrum matrix metalloproteinase inhibitor (10 μM GM6001; Calbiochem) did not decrease expansion by day 7 (data not shown). A 70–80% reduction in the amount of ECGS and heparin in the perfusing media led to decreased expansion but was accompanied by retraction of ECs and loss of confluence in both HUVEC and HDMEC tubes (data not shown). Thus, we conclude that expansion of tubes at days 3–7 does not require collagenases but does require a confluent endothelial lining.

By day 7, expanded tubes stabilize and can often persist for much longer without further expansion of lumenal diameters. In fact, some HUVEC tubes survived for 3 weeks before ECs began to detach from the walls of the collagen. HDMEC tubes remained morphologically stable for 2 weeks before the nuclei of the cells enlarged. We have not yet determined the mechanism for eventual failure of these tubes; senescence or prolonged mitogenic stimulation of ECs may play a role.

Permeability of endothelial tubes

One measure of normal microvascular function is a strong, reversible, and selective barrier function. To measure the permeability of HDMEC tubes, we perfused them with Alexa-Fluor-488-labeled BSA at days 3–4 or 6–7 (i.e., day 2 of confluence or day 5 of confluence). Time-lapse fluorescence microscopy indicated that very little BSA leaked into the surrounding collagen, even after 20 min of perfusion (Fig. 3, top
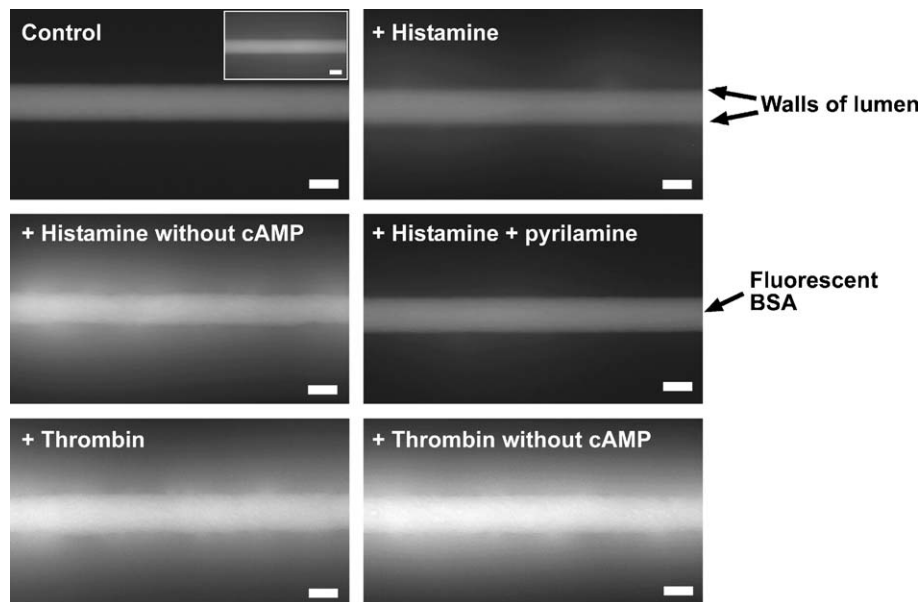

Fig. 3. Permeability of endothelial tubes in the absence and presence of histamine or thrombin. HDMEC tubes were perfused with labeled BSA, and fluorescence images after 20 min of perfusion are shown for a control tube (top left), a tube exposed to 100 μM histamine (top right), a tube exposed to 100 μM histamine in which dibutyryl cAMP was removed from the media 24 h prior (middle left), a tube exposed to 100 μM histamine and 100 μM pyrilamine (middle right), a tube exposed to 10 U/mL thrombin (lower left), and a tube exposed to 10 U/mL thrombin in which dibutyryl cAMP was removed 24 h prior (lower right). A control sample perfused with labeled 3 kDa dextran is shown in the inset of the top left image. The control sample and the sample pre-treated with pyrilamine exhibited strong barrier function to BSA; the barrier to 3 kDa dextran was weaker. Histamine greatly increased permeability in the absence of dibutyryl cAMP. Scale bars refer to 100 μm.

left, and Supplementary Movie 1), and EC tubes did not show any significant differences in permeability whether they had been at confluence for 2 or 5 days. The permeability coefficient of the BSA through the lumenal walls of the HDMEC tubes was estimated to be $5.5 \times 10^{-6} \pm 3.5 \times 10^{-6}$ cm/s ($n = 3$) at days 3–4 and $7.9 \pm 3.5 \times 10^{-6}$ cm/s at days 6–7 ($n = 3$, $P > 0.05$ by Wilcoxon's Sum of Ranks test). Most tubes exhibited small focal leaks of BSA that contributed to the variation in permeability between samples. When BSA was perfused through a collagen tube without cells, the collagen became nearly saturated with labeled protein within 20 min (data not shown). When a low molecular weight polysaccharide (Alexa-Fluor-488-labeled 3 kDa dextran) was perfused through an HDMEC tube, the dextran diffused out of the tube into the surrounding collagen more rapidly than the labeled BSA (Fig. 3; inset in top left image). Because our setup greatly reduces the convective contribution to flux, we were unable to determine the reflection coefficients to labeled solutes and thereby to quantify the selectivity of the barrier.

To determine whether the tubes could respond appropriately to agents known to perturb barrier function, we treated HDMEC tubes at day 3 or day 4 with histamine. In these samples, an increased amount of BSA diffused through the EC layer into the collagen (Fig. 3, top right, and Supplementary Movie 2). Removal of dibutyryl cAMP from the media 24 h prior to histamine treatment caused the EC layer to become extremely sensitive to histamine (Fig. 3, middle left, and Supplementary Movie 3). Time-lapse phase-contrast microscopy indicated that cell–cell junctions retracted upon addition of histamine, especially in the absence of dibutyryl cAMP (data not shown). Pre-treatment with saturating concentrations of pyrilamine (an H1 receptor antagonist) reduced permeability to near control levels in the presence of histamine (Fig. 3, middle right, and Supplementary Movie 4). Tubes exposed to thrombin were very permeable (Fig. 3, lower left and right, and Supplementary Movies 5 and 6); compared to ECs in tubes exposed to histamine, ECs in thrombin-treated tubes retracted to a much greater extent (data not shown).

Adhesion of leukocytes to endothelial tubes

To determine whether endothelial tubes could respond appropriately to inflammatory cytokines, we perfused HUVEC tubes at days 2–3 through days 6–7 (i.e., day 1 through 5 of confluence) with transformed neutrophil-like HL-60 cells with and without TNF-α. In the absence of exogenous TNF-α, densities of adherent HL-60 cells did not significantly differ among tubes, with 0.2 ± 0.3, 0.3 ± 0.5, 0.5 ± 0.6, 1.6 ± 1.3, and 0.4 ± 0.6 HL-60 cells/mm for days 2–3 through 6–7, respectively ($n = 3–5$ for each condition). Upon 4 h of treatment with TNF-α, however, the densities of adherent HL-60 cells increased significantly to 44.4 ± 10.7 adherent cells/mm ($n = 3$) for tubes at days 2–3. Adhesion was partially mediated by selectins and integrins: exposure of tubes to an antibody to E-selectin (clone 1.2B6) reduced the density of adherent cells to 18.1 ± 11.6 cells/mm ($n = 5$), while exposure to both antibodies to E-selectin and to the integrin CD18 (clone L130, added to

HL-60 cells prior to perfusion) further reduced the density of adherent cells to 7.3 ± 1.1 cells/mm ($n = 4$). Fig. 4 shows representative images of these tubes with adherent, fluorescently labeled HL-60 cells.

Endothelial tubes with diameters less than 120 μm

All tubes shown in Figs. 1–4 had initial diameters of 120 μm. To determine whether tubes with smaller initial diameters were viable, we repeated the procedure shown in Fig. 1 with needles that were etched so that their diameters were less than 120 μm. Immersion of 120-μm-diameter needles in a nickel etchant for various lengths of time yielded needles with diameters ranging from 30 to 95 μm, and these etched needles were used to make collagen tubes with HUVECs. In all cases, the inlet and outlet pressures were set at 16 and 11 cm H_2O, respectively. The length of etched portion of the tube was adjusted to hold τ at ~10 dyn/cm^2; that is, we kept tube length inversely proportional to tube radius since $\tau = \Delta Pr/2L$, where ΔP is the pressure difference across a tube, r is the radius of the tube, and L is the length of the tube. The smallest diameter tube that could be seeded and grown to confluence, and that sustained flow, was ~55 μm. When seeded in even narrower tubes, HUVECs appeared to grow in aggregates that spanned the lumen; flow in these samples was low, and the cells died within 3 days. Tubes with initial diameters of $\lesssim$55 μm invariably expanded by 25–35% (for example, initially 55-μm-diameter collagen tubes stabilized at 70–75 μm). Fig. 5 (top) shows a segment of a HUVEC tube that was created with a 55-μm-diameter needle.

In addition to cylindrical, narrowed endothelial tubes, etched needles can be used to create tubes with an abrupt change in diameter. Here, etching of the first ~4 mm at the tip of a needle yielded a non-cylindrical profile at the transition between etched and unetched areas. As shown in Fig. 5, a HUVEC tube made from a non-cylindrical needle expanded 25–35% in both the narrowed and full-diameter regions, with some smoothening at the transition point.

Tubes that incorporate perivascular cells

We incorporated perivascular cells into tubes two ways: by embedding PCs in the collagen prior to gelling or by seeding PCs into a confluent endothelial tube. To construct tubes with embedded PCs, we suspended ~10^5 PCs/mL in collagen; higher densities led to contraction of the collagen by PCs and delamination of collagen from the silicone housing. Because the long-term viability of PCs at 23°C is poor, we gelled the PC-containing collagen at 23°C for 10 min and then at 37°C for an additional 2 h. Previous studies have shown that a large fraction of collagen fibrils form during the short gelation at 23°C, leading to a final gel with properties similar to one gelled solely at 23°C (Wood and Keech, 1960). HDMECs that were seeded in tubes with embedded PCs did not appear to behave differently from those seeded in bare collagen tubes gelled at 23°C; contraction and invasion were consistently low, and tubes widened slightly after reaching confluence. PCs began to spread
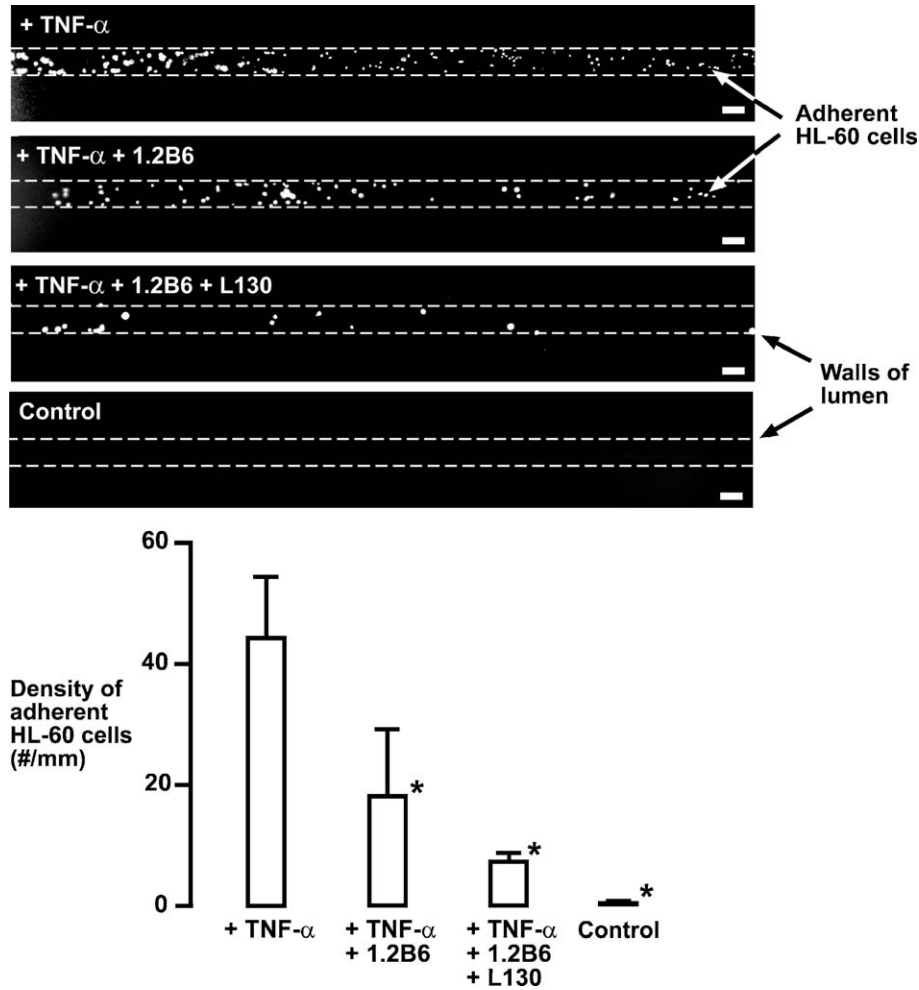
Fig. 4. Reactivity of endothelial tubes to TNF-α. Shown are fluorescence images of representative HUVEC tubes perfused with fluorescently labeled HL-60 cells after treatment with TNF-α (top), after treatment with TNF-α and the E-selectin antibody 1.2B6 (upper middle), after treatment with TNF-α and anti-E-selectin when the HL-60 cells were exposed to the CD18 antibody L130 (lower middle), and without any treatment (bottom). Data represent the average densities in 3–5 tubes. Asterisks (*) indicate that the data are significantly different compared to the TNF-α-only data. Scale bars refer to 100 μm.

within 1 day and became elongated and bipolar over the next few days. The barrier function of PC-containing HDMEC tubes weakened (Fig. 6 and Supplementary Movie 7); although the presence of PCs near the HDMEC monolayer did not appear to perturb the local barrier, the permeability coefficients increased to $P = 14.4 \pm 9.7 \times 10^{-6}$ cm/s ($n = 3$). Fig. 6 shows a
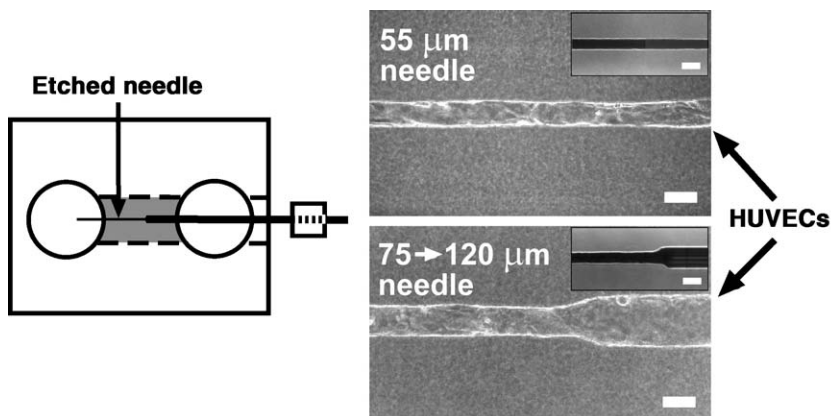

Fig. 5. Formation of endothelial tubes with diameters less than 120 μm. Needles were immersed in a nickel etchant to reduce their diameters to 30–95 μm. Phase-contrast images show a HUVEC tube made with a 55-μm-wide etched needle (top) and one made with a sharply tapering needle that transitions from 120 μm to 75 μm (bottom). Insets display images of the needles used to make these channels. Scale bars refer to 100 μm.
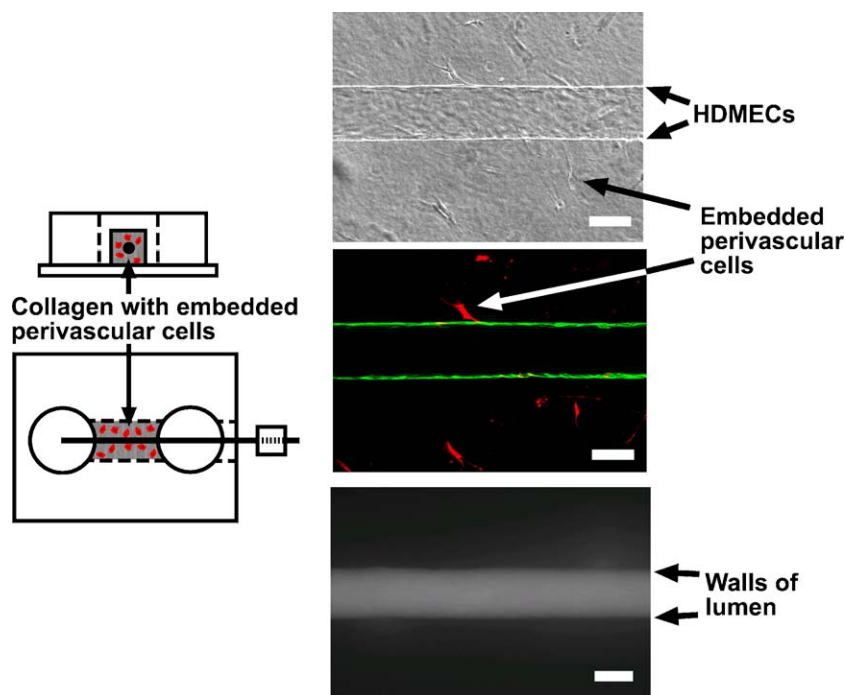
Fig. 6. Formation of tubes that incorporate HDMECs and PCs. A phase-contrast image (top) and a corresponding fluorescence image of the center plane of the tube with perivascular cells embedded within the collagen matrix (middle) are shown. PCs were labeled with CellTracker Red prior to seeding; HDMECs were fixed and stained with an antibody to CD31 plus a secondary antibody (Alexa Fluor 488 goat anti-mouse antibody; green). The bottom picture shows the fluorescence image after 20 min of perfusion with fluorescently labeled BSA; in this sample, PCs were not labeled. Scale bars refer to 100 μm.

fluorescence image of an HDMEC tube with embedded PCs that was stained for the endothelial-specific marker CD31 (PECAM-1); the continuity of fluorescence demonstrates that the EC layer is intact and complete (at least in the regions that were imaged).

To construct tubes with PCs seeded into the lumen, we allowed HDMECs to grow to confluence and then introduced a suspension of PCs into these tubes. The few PCs that attached extravasated through the EC layer into the collagen. Once they resided within the collagen, PCs migrated randomly and did not appear to favor a location near ECs.

Discussion

Using microvascular cells and collagen, we have created single long tubes that exhibited long-term barrier function and reactivity to cytokines. These tubes consisted of ECs that were seeded on the lumenal surface of collagen tubes molded around stainless steel needles. Perfusion of these tubes allowed ECs to grow to confluence and form a quiescent but reactive monolayer that persisted for at least 5 days post-confluence and often for much longer. Because the collagen gels were formed with open channels already present, perfusion could commence immediately after seeding of ECs. The presence of constant flow in these tubes enhanced survival of ECs; in fact, elimination of flow by deliberate constriction of the tubing led to rapid breakdown of EC monolayers (data not shown).

Both HUVEC and HDMEC tubes of a variety of initial diameters did not retain their initial geometries perfectly and exhibited similar types of deformations. These deformations developed at characteristic times, with initial contraction (days 1–2) followed by invasion (days 2–3) and expansion (days 3–7). By systematically varying the gelling temperature and collagen concentration, we determined that 6.5 mg/mL gels formed at ≤23°C led to tubes that minimized contraction and invasion. We have not yet isolated conditions that enable perfusion at ~10 cm H_2O without enlargement. After day 7, tubes stabilized at final diameters ranging from 75 to 150 μm (i.e., 25–35% enlargement).

Once confluent (days 2–3), both HUVEC and HDMEC tubes exhibited normal microvascular functions. In particular, these tubes displayed three behaviors important for studies of inflammation: First, these tubes possessed a strong barrier, with an estimated permeability for albumin of $5.5 \times 10^{-6} \pm 3.5 \times 10^{-6}$ cm/s at day 2, which is slightly higher than that of intact or explanted mammalian venules in vivo (Wu et al., 2001; Curry and Joyner, 1988; Turner and Pallone, 1997). Second, the EC monolayers that lined these tubes did not normally support the adhesion of leukocytes. Third, tubes responded to inflammatory mediators (histamine, thrombin, and TNF-α) by increasing permeability and enhancing adhesion of leukocytes. These functional changes followed classical pathways and could be inhibited by antagonists to the H1 histamine receptor and/or by addition of a cAMP analog (for barrier function) and by addition of antibodies to E-selectin and CD18 integrin (for leukocyte adhesion).

Strangely, the permeability of HDMEC tubes reached a steady state by day 2 of confluence. Previous studies in vitro have shown that static monolayers of ECs are initially leaky and

gradually reduce their permeabilities over the span of 5–10 days (Casnocha et al., 1989; Albelda et al., 1988). Constant perfusion in our tubes may enhance barrier function by enhancing the delivery of albumin to the ECs (Lum et al., 1991; Huxley and Curry, 1991). In support of this possibility, sheared monolayers of ECs reach a minimum in permeability upon reaching confluence (Jo et al., 1991). Even at steady state, HDMEC tubes exhibit focal leaks (1–3 leaks/mm); these leaks may result from endothelial gaps that normal post-capillary venules possess in vivo (McDonald, 1994).

We have also observed that the presence of perivascular cells *increases* permeability, although this increase did not reach statistical significance. Signals derived from PCs are required to form non-leaky microvessels in vivo (Yancopoulos et al., 2000; von Tell et al., 2005). Since PCs in our tubes do not reside in a peri-endothelial location even if they were originally placed there, the ECs in tubes may not be exposed to these PC-derived signals in sufficient amounts to lower permeability (Morikawa et al., 2002).

The major advantages of these EC tubes over other in vitro models are that the ECs in tubes are constantly perfused and reside on a biologically relevant and porous matrix and that the tubes mimic the scale and 3D cellular organization of microvessels in vivo. Many microvascular behaviors, such as diapedesis, metastasis, and loss of barrier function, inherently require the delivery of materials (cells or labeled molecules) selectively through the lumens of tubes. Such delivery has not been demonstrated in spontaneously organized tubes of ECs (Montesano et al., 1983; Darland and D'Amore, 2001; Ueda et al., 2004) but is straightforward to implement in our tubes. Likewise, these behaviors require a porous matrix under the EC monolayers through which cells or labeled molecules can escape. Cultures of microvascular cells on tissue culture plates do not satisfy this requirement, although it may be possible to construct a parallel-plate system to expose ECs on a gel to shear (following the strategy outlined in Ueda et al., 2004). The ability to image the walls of an endothelial layer in real time in our tubes greatly simplifies measurements of permeability and cellular adhesion over time. Our structures blur the distinction between in vitro cultures and in vivo tissues and provide a method to produce microvascular tubes for studies of the inflammatory response.

Compared with exteriorized microvascular beds and single explanted microvessels, our microvascular tubes clearly lack a well-organized mural coat and thus cannot be used for studies of vasomotion, vasodilation, or vasoconstriction. Nevertheless, we believe these in vitro models provide some advantages in time, cost, and convenience over in vivo techniques. Unlike in vivo or ex vivo preparations (Kaul et al., 1989; Kulkarni et al., 1994; Menger and Lehr, 1993), these in vitro tubes can be perfused for several days and are readily transferred to and from the microscope for repeated imaging. Perhaps most importantly, these tubes are highly reproducible in shape and length and avoid the natural variation of vessels in vivo. We have begun to use this reproducibility to generate large-scale arrays of microvascular tubes for screening agents that can perturb microvascular function.

An additional difference with in vivo microvessels is the lack of lymphatic drainage in our system. The silicone housing that surrounds the in vitro tubes exhibit a low permeability to water vapor (McDonald and Whitesides, 2002; Randall and Doyle, 2005). Convective transport of solutes is essentially negligible in the tubes. Since proteins can diffuse into the gel before confluence is reached but cannot escape easily when the barrier is established, the "interstitial" fluid will contain high concentrations of protein, a situation analogous to lymphatic blockage in vivo (Saharinen et al., 2004). We are currently examining the behavior of constructs in which a second empty tube serves as drainage to lower interstitial pressure and interstitial protein concentrations.

We have not yet observed the deposition of a well-organized basement membrane in these tubes. In HDMEC tubes, the lack of basement membrane may reflect the presence of lymphatic ECs in these cultures; lymphatic vessels generally have little to no basement membrane (Saharinen et al., 2004). In HUVEC tubes, the reason for basement membrane deficiency is unclear. Given that mitogens often enhance the proteolytic activity of HUVECs (including the secretion of collagenases capable of degrading basement membrane), we suspect that reducing the amount of growth factors in perfusate may help ECs to deposit and assemble a basement membrane (Pepper et al., 1990). Addition of factors such as transforming growth factor-β, which promotes maturation of vessels and matrix deposition, may also promote formation of basement membrane.

Despite these differences with microvessels in vivo, endothelial tubes appear to faithfully reproduce several functions and perfusion conditions of large venules. The final diameters of these tubes (75–150 μm) approximate those of collecting venules (Simionescu and Simionescu, 1984). The flow conditions we chose mimicked those of venules in vivo, which experience shear stresses of 10–40 dyn/cm^2 (Nerem, 1981) and lumenal pressures that range from 25 mm Hg down to nearly zero (Ganong, 2001). Given that the endothelial tubes exhibit inflammatory responses that are similar to those of native venules, we believe that these tubes will serve as useful in vitro models of inflammation under constant perfusion.

These tubes may also model so-called "giant" capillaries that are observed in tumors or sites of chronic inflammation (Warren et al., 1978; Monticone et al., 2000; Vayssairat et al., 1998). These vessels have little or no pericytic coat and scant basement membrane and often exist in tissues that have high interstitial fluid pressures; they may represent the most accurate analog in vivo of the EC tubes.

The methods described here are not limited to tubes of human ECs (HUVECs and HDMECs) in rat tail-derived collagen. For instance, we have successfully formed tubes within a mixture of rat tail collagen and Matrigel, within bovine skin collagen (Vitrogen), and within fibrin. Likewise, non-human ECs (bovine pulmonary artery ECs and bovine lung microvascular ECs) can be readily incorporated in these models. Even non-endothelial cell types, such as human renal epithelial cells, will grow to confluence in these tubes (data not shown). Thus, these methods may be useful in the study of both endothelial and epithelial physiology.

Acknowledgments

Appendix A. Supplementary data

Supplementary data associated with this article can be found in the online version at doi:10.1016/j.mvr.2006.02.005.

References

Albelda, S.M., et al., 1988. Permeability characteristics of cultured endothelial cell monolayers. J. Appl. Physiol. 64, 308–322.

Casnocha, S.A., et al., 1989. Permeability of human endothelial monolayers: effect of vasoactive agonists and cAMP. J. Appl. Physiol. 67, 1997–2005.

Chamley-Campbell, J., et al., 1979. The smooth muscle cell in culture. Physiol. Rev. 59, 1–61.

Collins, S.J., et al., 1978. Terminal differentiation of human promyelocytic leukemia cells induced by dimethyl sulfoxide and other polar compounds. Proc. Natl. Acad. Sci. U. S. A. 75, 2458–2462.

Collins, P.W., et al., 1993. von Willebrand factor release and P-selectin expression is stimulated by thrombin and trypsin but not IL-1 in cultured human endothelial cells. Thromb. Haemostasis 70, 346–350.

Coughlin, S.R., 2000. Thrombin signalling and protease-activated receptors. Nature 407, 258–264.

Crow, E.L., et al., 1960. Statistics Manual. Dover Publications, New York.

Curry, F.E., Joyner, W.L., 1988. Modulation of capillary permeability: methods and measurements in individually perfused mammalian and frog microvessels. In: Ryan, U.S. (Ed.), Endothelial Cells. CRC Press, pp. 3–18.

Darland, D.C., D'Amore, P.A., 2001. TGF beta is required for the formation of capillary-like structures in three-dimensional cocultures of 10T1/2 and endothelial cells. Angiogenesis 4, 11–20.

Folkman, J., et al., 1979. Long-term culture of capillary endothelial cells. Proc. Natl. Acad. Sci. U. S. A. 76, 5217–5221.

Ganong, W.F., 2001. Review of medical physiology. In: Foltin, J., Mantragrano, J., Ransom, J., Davis, K. (Eds.), Lange Medical Books. McGraw-Hill Medical.

Gao, K.X., Godkin, J.D., 1991. A new method for transfer of polyethylene glycol-embedded tissue sections to silanated slides for immunocytochemistry. J. Histochem. Cytochem. 39, 537–540.

Gitlin, J.D., D'Amore, P.A., 1983. Culture of retinal capillary cells using selective growth media. Microvasc. Res. 26, 74–80.

Groger, M., et al., 2004. IL-3 induces expression of lymphatic markers Prox-1 and podoplanin in human endothelial cells. J. Immunol. 173, 7161–7169.

Hauert, A.B., et al., 2002. Differentiated HL-60 cells are a valid model system for the analysis of human neutrophil migration and chemotaxis. Int. J. Biochem. Cell Biol. 34, 838–854.

Holtham, K.A., Slepecky, N.B., 1995. A simplified method for obtaining 0.5-microns sections of small tissue specimens embedded in PEG. J. Histochem. Cytochem. 43, 637–643.

Huxley, V.H., Curry, F.E., 1991. Differential actions of albumin and plasma on capillary solute permeability. Am. J. Physiol. 260, H1645–H1654.

Huxley, V.H., et al., 1987. Quantitative fluorescence microscopy on single capillaries: alpha-lactalbumin transport. Am. J. Physiol. 252, H188–H197.

Jalali, S., et al., 2001. Integrin-mediated mechanotransduction requires its dynamic interaction with specific extracellular matrix (ECM) ligands. Proc. Natl. Acad. Sci. U. S. A. 98, 1042–1046.

Jo, H., et al., 1991. Endothelial albumin permeability is shear dependent, time dependent, and reversible. Am. J. Physiol. 260, H1992–H1996.

Kaul, D.K., et al., 1989. Microvascular sites and characteristics of sickle cell adhesion to vascular endothelium in shear flow conditions: pathophysiological implications. Proc. Natl. Acad. Sci. U. S. A. 86, 3356–3360.

Klosen, P., et al., 1993. PEG embedding for immunocytochemistry: application to the analysis of immunoreactivity loss during histological processing. J. Histochem. Cytochem. 41, 455–463.

Kriehuber, E., et al., 2001. Isolation and characterization of dermal lymphatic and blood endothelial cells reveal stable and functionally specialized cell lineages. J. Exp. Med. 194, 797–808.

Kulkarni, P., et al., 1994. A novel method to assess reactivities of retinal microcirculation. Microvasc. Res. 48, 39–49.

Kvietys, P.R., Granger, D.N., 1997. Endothelial cell monolayers as a tool for studying microvascular pathophysiology. Am. J. Physiol. 273, G1189–G1199.

Lum, H., et al., 1991. Serum albumin decreases transendothelial permeability to macromolecules. Microvasc. Res. 42, 91–102.

Madri, J.A., et al., 1988. Phenotypic modulation of endothelial cells by transforming growth factor-beta depends upon the composition and organization of the extracellular matrix. J. Cell Biol. 106, 1375–1384.

McDonald, D.M., 1994. Endothelial gaps and permeability of venules in rat tracheas exposed to inflammatory stimuli. Am. J. Physiol. 266, L61–L83.

McDonald, J.C., Whitesides, G.M., 2002. Poly(dimethylsiloxane) as a material for fabricating microfluidic devices. Acc. Chem. Res. 35, 491–499.

Menger, M.D., Lehr, H.A., 1993. Scope and perspectives of intravital microscopy-bridge over from in vitro to in vivo. Immunol. Today 14, 519–522.

Montesano, R., Orci, L., 1985. Tumor-promoting phorbol esters induce angiogenesis in vitro. Cell 42, 469–477.

Montesano, R., et al., 1983. In vitro rapid organization of endothelial cells into capillary-like networks is promoted by collagen matrices. J. Cell Biol. 97, 1648–1652.

Monticone, G., et al., 2000. Quantitative nailfold capillary microscopy findings in patients with acrocyanosis compared with patients having systemic sclerosis and control subjects. J. Am. Acad. Dermatol. 42, 787–790.

Morikawa, S., et al., 2002. Abnormalities in pericytes on blood vessels and endothelial sprouts in tumors. Am. J. Pathol. 160, 985–1000.

Moy, A.B., et al., 1993. The effect of histamine and cyclic adenosine monophosphate on myosin light chain phosphorylation in human umbilical vein endothelial cells. J. Clin. Invest. 92, 1198–1206.

Neil, M.A.A., et al., 1997. Method of obtaining optical sectioning by using structured light in a conventional microscope. Opt. Lett. 22, 1905–1907.

Nerem, R.M., 1981. Arterial fluid dynamics and interactions with the vessel walls. In: Schwartz, C.J., Werthessen, N.T., Wolf, S. (Eds.), Structure and Function of the Circulation. Plenum Publishing Corp., New York.

Neumann, T., et al., 2003. Tissue engineering of perfused microvessels. Microvasc. Res. 66, 59–67.

Pepper, M.S., et al., 1990. Transforming growth factor-beta 1 modulates basic fibroblast growth factor-induced proteolytic and angiogenic properties of endothelial cells in vitro. J. Cell Biol. 111, 743–755.

Podgrabinska, S., et al., 2002. Molecular characterization of lymphatic endothelial cells. Proc. Natl. Acad. Sci. U. S. A. 99, 16069–16074.

Randall, G.C., Doyle, P.S., 2005. Permeation-driven flow in poly(dimethylsiloxane) microfluidic devices. Proc. Natl. Acad. Sci. U. S. A. 102, 10813–10818.

Richard, L., et al., 1998. A simple immunomagnetic protocol for the selective isolation and long-term culture of human dermal microvascular endothelial cells. Exp. Cell Res. 240, 1–6.

Saharinen, P., et al., 2004. Lymphatic vasculature: development, molecular regulation and role in tumor metastasis and inflammation. Trends Immunol. 25, 387–395.

Simionescu, M., Simionescu, N., 1984. Ultrastructure of the microvascular wall: functional correlations. In: Renkin, E.M., Michel, C.C. (Eds.), Handbook of Physiology, Section 2: The Cardiovascular System. American Physiological Society, Bethesda.

Turner, M.R., Pallone, T.L., 1997. Hydraulic and diffusional permeabilities of isolated outer medullary descending vasa recta from the rat. Am. J. Physiol. 272, H392–H400.

Ueda, A., et al., 2004. Effect of shear stress on microvessel network formation of endothelial cells with in vitro three-dimensional model. Am. J. Physiol.: Heart Circ. Physiol. 287, 994–1002.

Vayssairat, M., et al., 1998. Clinical significance of subcutaneous calcinosis in patients with systemic sclerosis. Does diltiazem induce its regression? Ann. Rheum. Dis. 57, 252–254.

von Tell, D., et al., 2005. Pericytes and vascular stability. Exp. Cell Res 623–629.

Warren, B.A., et al., 1978. Metastasis via the blood stream: the method of intravasation of tumor cells in a transplantable melanoma of the hamster. Cancer Lett. 4, 245–251.

Weinberg, C.B., Bell, E., 1986. A blood vessel model constructed from collagen and cultured vascular cells. Science 231, 397–400.

Williams, B.R., et al., 1978. Collagen fibril formation. Optimal in vitro conditions and preliminary kinetic results. J. Biol. Chem. 253, 6578–6585.

Wood, G.C., Keech, M.K., 1960. The formation of fibrils from collagen solutions: 1. The effect of experimental conditions: kinetic and electron-microscope studies. Biochem. J. 75, 588–598.

Wu, M.H., et al., 2001. Integrin binding to fibronectin and vitronectin maintains the barrier function of isolated porcine coronary venules. J. Physiol. 532, 785–791.

Yancopoulos, G.D., et al., 2000. Vascular-specific growth factors and blood vessel formation. Nature 407, 242–248.

Yuan, Y., et al., 1992. Flow modulates coronary venular permeability by a nitric oxide-related mechanism. Am. J. Physiol. 263, H641–H646.

Yuan, Y., et al., 1993. Permeability to albumin in isolated coronary venules. Am. J. Physiol. 265, H543–H552.